Electronic Supplementary Material (ESI) for Journal of Materials Chemistry A.

Supplementary Information

A silicon-based hybrid photocathode modified with an N_5-chelated nickel catalyst in a noble-metal-free biomimetic photoelectrochemical cell for solar-driven unbiased overall water splitting

Lunlun Gong, Peili Zhang, Guoquan Liu, Yu Shan and Mei Wang*

State Key Laboratory of Fine Chemicals, Dalian University of Technology, Dalian 116024, China

*Corresponding author. E-mail: symbueno@dlut.edu.cn

Additional experimental

Materials and instruments

The planar p-Si wafers (P-100, 10–20 Ω cm, 500 μm) were purchased from Hangzhou Bojing Science and Technology Limited Company. TiO_2 pastes (DHS-TPP3, 20 nm, anatase) used for doctor blading were purchased from Dalian Heptachroma Solartech Limited Company and stored at 5 °C, and Nafion membranes (N117) from DuPont. Methyl 4-(bromomethyl)benzoate, 2-(chloromethyl)pyridine hydrochloride, lithium bis(trimethylsilyl)amide (LHMDS, 1 M in THF), and *O*-benzylhydroxylamine were purchased from Energy Chemical, and tetrakis(dimethylamido)titanium(IV) (TDMAT) and Pd/C (10 wt.%) from J&K Scientific Limited Company. Compounds $Ni(BF_4)_2{\cdot}6H_2O$, $Co(BF_4)_2{\cdot}6H_2O$, $Co(NO_3)_2{\cdot}6H_2O$, $CoCl_2{\cdot}6H_2O$, hydroxylammonium chloride, ethyl isonicotinate, and dimethylglyoxime were purchased from Aladdin Industrial Corporation. Butoxyacetic acid was purchased from Shanghai Shaoyuan Limited Company, and 4-*tert*-butylpyridine from Bide Pharmatech. Other reagents and solvents were purchased from local suppliers. Unless otherwise specified, all reagents were analytically pure and used without further purification. Complex $CoPy^{HA}$ was prepared according to our previously reported procedure.[S1] The water used in the synthesis experiments and PEC measurements was deionized with a Millipore AFS-E system (18.2 MΩ cm resistivity).

The ^1H NMR spectra were recorded on a 400 MHz/500 MHz system (Bruker AVANCE II 400/III 500). Mass spectra (MS) were measured on an LTQ Orbitrap XL mass spectrometer from Thermo Fisher Scientific Inc. and a Q-TOF Micro System from Micromass UK Limited. Field-emission SEM images were measured on a Nova NanoSEM 450 instrument. The XPS spectra of the photoelectrodes were collected on a Thermo VG ESCALAB 250 surface analysis system. The ATR-FTIR spectra were measured on a Thermo Fisher Nicolet iN10 spectrometer. The ICP-OES data of the loading amounts of molecular catalysts were analyzed

on a PerkinElmer 2000 DV system. UV−vis spectra of the molecular catalysts were obtained from a Lambda 35 instrument (PerkinElmer).

Preparation of Hydroxamate-Functionalized N_5-Ligand (N_5)^{HA}

The hydroxamate-functionalized diamine-tripyridine N_5-ligand was synthesized by referring to the literature procedure.[S2,S3] In our synthesis, methyl 4-(bromomethyl)benzoate was used as a starting reagent to replace bromomethylbenzene used in the literature, and finally the ester group was converted to the hydroxamate group (Fig. S1).

Compound 1. Methyl 4-(bromomethyl)benzoate (25 g, 110 mmol) was slowly added to the ethanol solution (180 mL) containing ethylenediamine (14.74 mL, 220 mmol) under reflux, and then the mixture was stirred for 18 h. After that, the insoluble solid was filtered out, and the oily substance was collected by removing the filtrate using a rotary evaporator. A NaCl-saturated aqueous solution was added, and the obtained substance was extracted three times using chloroform. The organic phases obtained was then dried by using anhydrous Na_2SO_4. After Na_2SO_4 was filtered out, the organic solvents were evaporated from the filtrate, and the product was purified by column chromatography using CH_2Cl_2/CH_3OH as eluent, giving a yield of 28% (6.5 g). ^{1}H NMR (500 MHz, $CDCl_3$): δ 2.69 (t, J = 5.8 Hz, 2H, CH_2), 2.82 (t, J = 5.8 Hz, 2H, CH_2), 3.86 (d, J = 9.3 Hz, 2H, CH_2), 3.90 (s, 3H, CH_3), 7.39 (t, J = 8.1 Hz, 2H, Ph), 7.96–8.03 (m, 2H, Ph). ESI-MS: calcd for $C_{11}H_{16}N_2O_2$, $[M+H]^+$: *m/z* 209.12; found for $[M+H]^+$: *m/z* 209.14 (Fig. S2).

Compound 2. 2-(Chloromethyl)pyridine hydrochloride (11 g, 67 mmol) was added to an aqueous solution of NaOH (3.3 g, 82.5 mmol) under stirring. After being stirred for 15 min, the solution was extracted three times with dichloromethane, and then the organic extract was dried by using anhydrous Na_2SO_4. The 2-(chloromethyl)pyridine was collected in a quantitative yield after filtration of Na_2SO_4 and evaporation of organic solvent. Then compound **1** (4.71 g, 22.6 mmol) and 2-(chloromethyl)pyridine (8.5 g, 67 mmol) were added

to a mixed solvent containing ultra dry acetonitrile (70 mL), dichloromethane (40 mL) and *N*,*N*-dimethylformamide (30 mL). After the above solution was stirred for 15 min, the potassium carbonate (11.5 g, 83.2 mmol) was added, and then the solution was stirred at 90 °C for 24 h. The oily product was obtained after filtration of insoluble solid followed by evaporation of the organic solvents from the filtrate. The crude product was dissolved in boiling diethyl ether, and the solid residue was filtered out again. The filtrate was cooled to room temperature, and the brown oil was obtained after the ether solvent was removed. Finally, the product was purified by column chromatography with CH_2Cl_2/CH_3OH as eluent. Yield: 29% (3.2 g). ^{1}H NMR (400 MHz, CD_3OD): δ 2.66 (tt, J = 10.5 Hz, 5.2 Hz, 4H, $2CH_2$), 3.60 (d, J = 7.0 Hz, 2H, CH_2), 3.70 (d, J = 14.2 Hz, 6H, $3CH_2$), 3.89 (s, 3H, CH_3), 7.22–7.29 (m, 3H, Py), 7.38 (d, J = 8.2 Hz, 2H, Ph), 7.51 (dd, J = 14.3 Hz, 7.9 Hz, 3H, Py), 7.68–7.77 (m, 3H, Py), 7.87 (d, J = 8.2 Hz, 2H, Ph), 8.36–8.42 (m, 3H, Py). ESI-MS: calcd for $C_{29}H_{31}N_5O_2$, $[M+H]^+$: *m/z* 482.25; found for $[M+H]^+$: *m/z* 482.28 (Fig. S3).

Compound 3. Compound **2** (1.07 g, 2.2 mmol) and *O*-benzylhydroxylamine (273 μL, 2.3 mmol) were added to ultra dry tetrahydrofuran (100 mL) under N_2 atmosphere. After 20 min of deaeration with bubbling, LHMDS (7.14 mL, 7.14 mmol) was added dropwise to the above solution, and the solution was stirred at room temperature for 10 h. Thereafter, the reaction was quenched by adding NH_4Cl-saturated aqueous solution. The resulting solution was extracted three times with ethyl acetate, and then the organic phase obtained was dried with anhydrous $MgSO_4$. After $MgSO_4$ was filtered out, the oily product was collected by evaporating the organic solvents from the filtrate. The product was obtained as a yellow-brown oil by column chromatography using CH_2Cl_2/CH_3OH as eluent. Yield: 71% (0.9 g). ^{1}H NMR (400 MHz, DMSO-d_6): δ 2.51–2.72 (m, 4H, $2CH_2$), 3.49–3.80 (m, 8H, $4CH_2$), 4.92 (s, 2H, CH_2), 7.19–7.25 (m, 3H, Ph), 7.31–7.43 (m, 8H, Ph (4H) and Py (4H)), 7.46 (d, J = 6.8 Hz, 2H, Ph), 7.67 (ddd, J = 20.3 Hz, J = 11.7 Hz, J = 4.6 Hz, 5H, Py), 8.44 (d,

J = 4.4 Hz, 3H, Py), 11.71 (s, 1H, NH). ESI-MS: calcd for $C_{35}H_{36}N_6O_2$, $[M+H]^+$: *m/z* 573.29; found for $[M+H]^+$: *m/z* 573.07 (Fig. S4).

***Ligand* $(N_5)^{HA}$.** Compound **3** (200 mg, 0.35 mmol) was dissolved in ultra dry methanol (10 mL). After the above solution was stirred for 10 min, Pd/C (150 mg, 10 wt.%) was added to the solution. The mixture was stirred for 40 h at room temperature under H_2 atmosphere. Afterward, Pd/C was filtered out by using diatomite. The product was obtained as a faint yellow oil by removing the remaining organic solvents from the filtrate with a rotary evaporator. Yield: 83% (140 mg). ^{1}H NMR (400 MHz, CD_3OD): δ 3.10 (dt, *J* = 50.1 Hz, 5.7 Hz, 4H, $2CH_2$), 3.89 (d, *J* = 13.9 Hz, 4H, $2CH_2$), 4.02 (s, 4H, $2CH_2$), 7.25–7.52 (m, 8H, Ph (2H) and Py (6H)), 7.75 (q, *J* = 8.0 Hz, 3H, Py), 7.85 (d, *J* = 8.0 Hz, 2H, Ph), 8.48 (dd, *J* = 39.0 Hz, *J* = 4.5 Hz, 3H, Py). ESI-MS: calcd for $C_{28}H_{30}N_6O_2$, $[M+H]^+$: *m/z* 483.24; found for $[M+H]^+$: *m/z* 483.03 (Fig. S5).

Preparation of $Ni(N_5)^{HA}$

Compounds $Ni(BF_4)_2{\cdot}6H_2O$ (31.5 mg, 0.092 mmol) and ligand $(N_5)^{HA}$ (45 mg, 0.092 mmol) were dissolved in a mixed solvent containing acetone (8 mL) and water (12 mL) at room temperature under N_2 atmosphere. The solution was stirred for 16 h at room temperature. After the organic solvent was evaporated, the pale-brown solid product was collected, which was recrystallized in the ether/methanol solution. Yield: 70% (47 mg). TOF-MS: calcd for $[M^{2+}-H_2O]^{2+}$: *m/z* 270.09; found for $[M^{2+}-H_2O]^{2+}$: *m/z* 269.92 (Fig. S6).

Preparation of $Co(N_5)^{HA}$

Ligand $(N_5)^{HA}$ (45.0 mg, 0.092 mmol) was dissolved in a mixed solvent of acetone (8 mL) and water (12 mL) under N_2 atmosphere. After 30 min of deaeration with bubbling, $Co(BF_4)_2{\cdot}6H_2O$ (31.4 mg, 0.092 mmol) was added to the above solution. The following process was the same as that for the preparation of $Ni(N_5)^{HA}$. The light-pink product was obtained with recrystallization of the solid residue in the ether/methanol solution under N_2

atmosphere. Yield: 73% (49 mg). TOF-MS: calcd for $[M^{2+}-H_2O]^{2+}$: *m*/*z* 270.59; found for $[M^{2+}-H_2O]^{2+}$: *m*/*z* 270.66 (Fig. S7).

Preparation of Co_4O_4-OC_4H_9

Molecular catalyst Co_4O_4-OC_4H_9 was prepared by referring to the previously reported procedure,[S4] but the pyridine ligand was replaced by 4-*tert*-butylpyridine. ^{1}H NMR (400 MHz, CD_3CN): δ 0.83 (t, J = 7.3 Hz, 12H), 1.25 (s, 36H), 1.28 (s, 8H), 1.37–1.46 (m, 8H), 3.39 (ddd, J = 15.7 Hz, 8.9 Hz, 2.1 Hz, 8H), 3.77−4.03 (m, 8H), 7.16 (d, J = 6.3 Hz, 8H), 8.36 (d, J = 6.3 Hz, 8H). ESI-MS: calcd for $C_{60}H_{96}Co_4N_4O_{16}$, $[M+H]^+$: *m*/*z* 1365.41; found for $[M+H]^+$: *m*/*z* 1365.54 (Fig. S26).

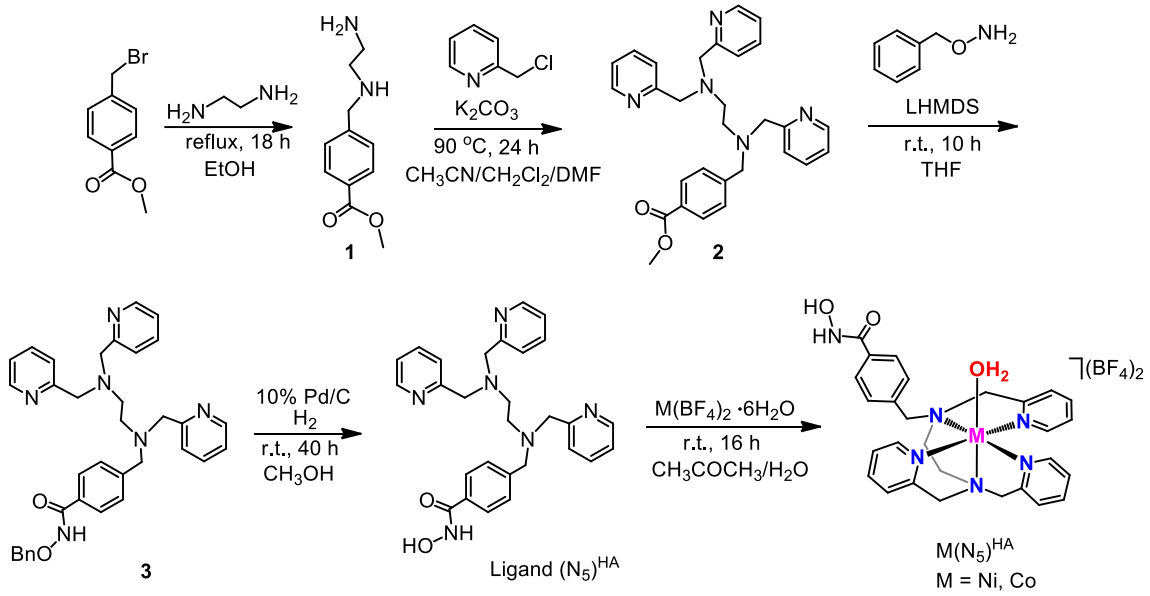

Fig. S1 Preparation routes for the diamine-tripyridine ligand and complexes $M(N_5)^{HA}$ (M = Ni, Co).

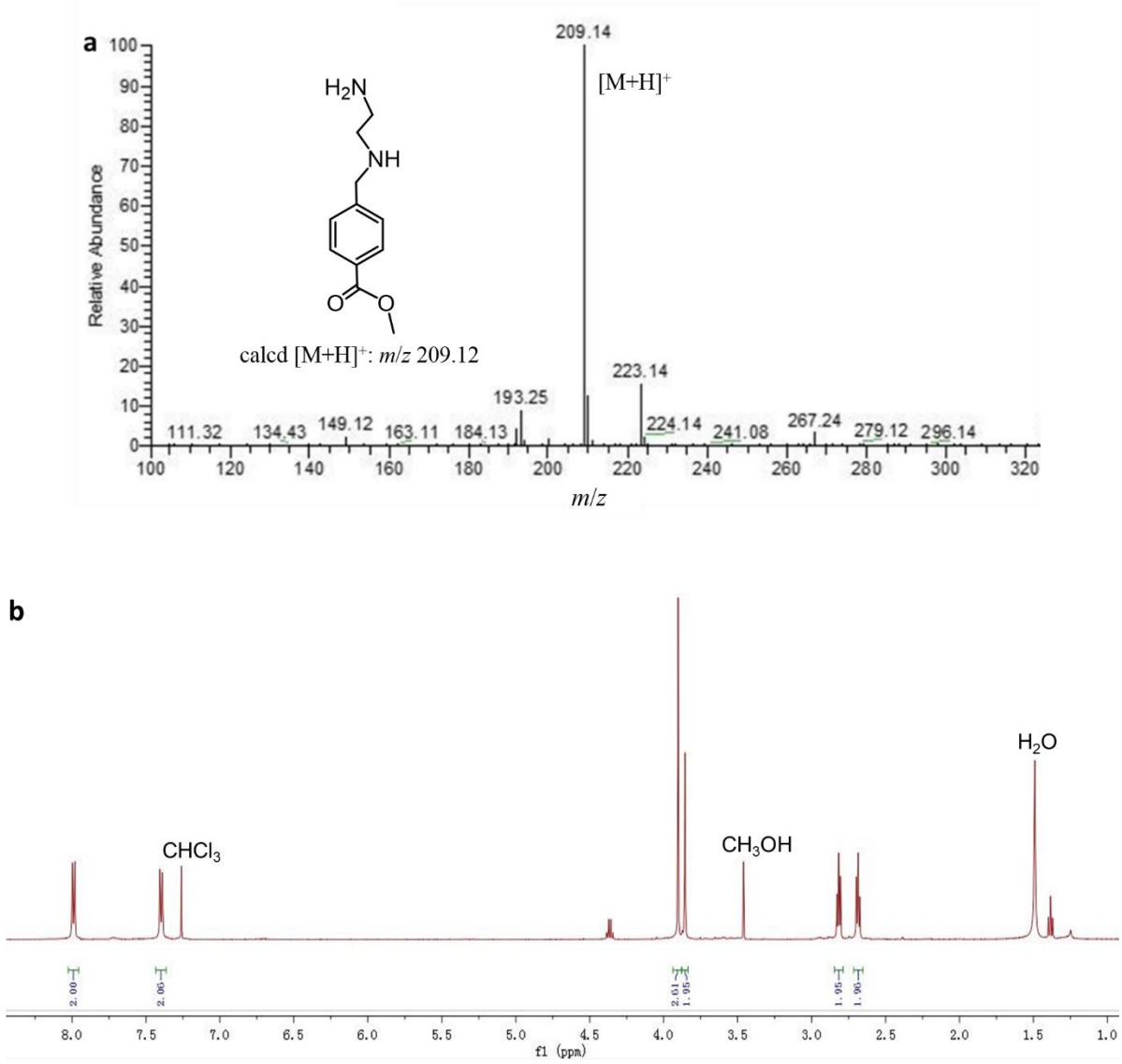

Fig. S2 (a) Mass spectrum and (b) ^{1}H NMR spectrum for product **1** in $CDCl_3$.

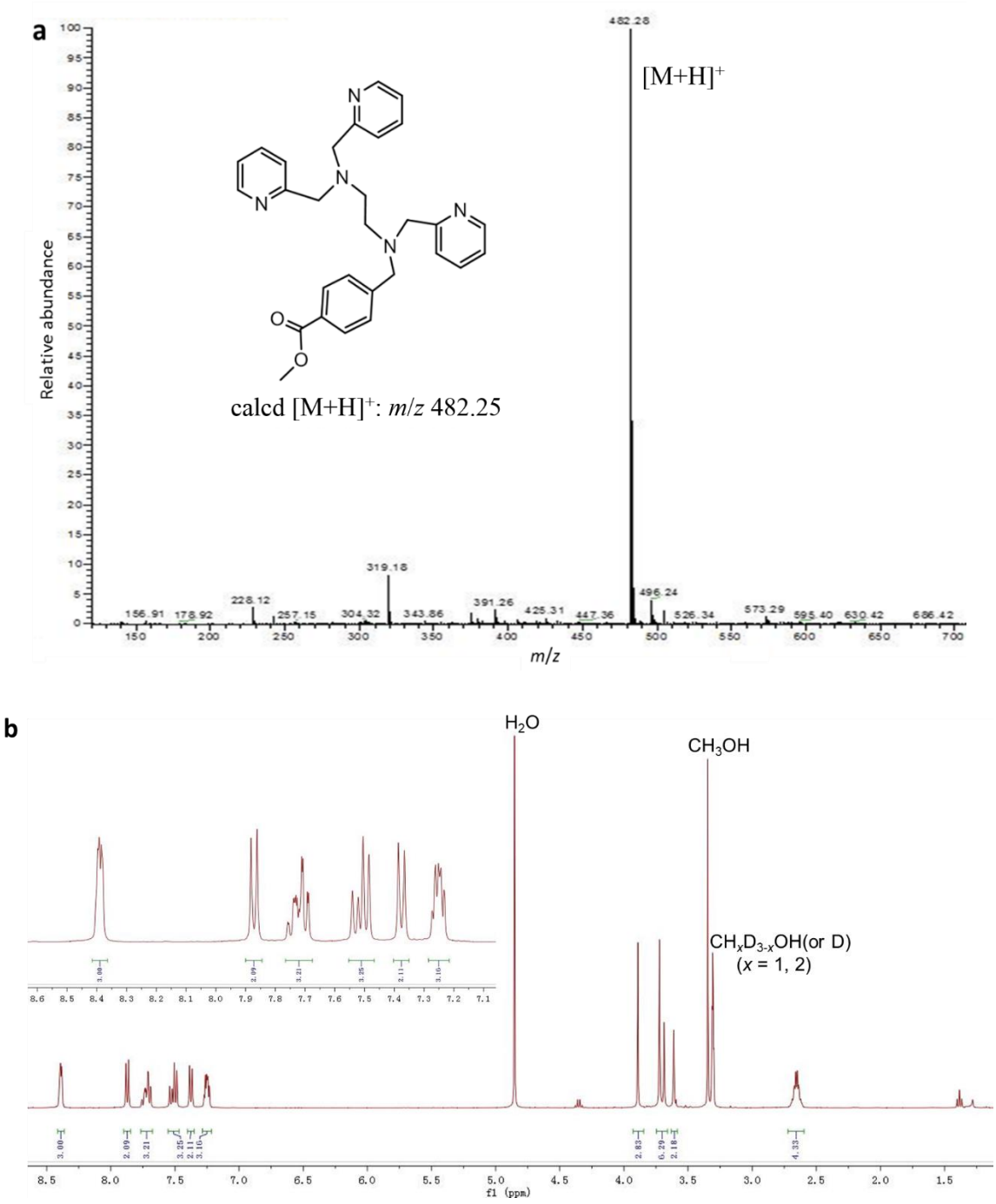

Fig. S3 (a) Mass spectrum and (b) ^{1}H NMR spectrum for product **2** in CD_3OD.

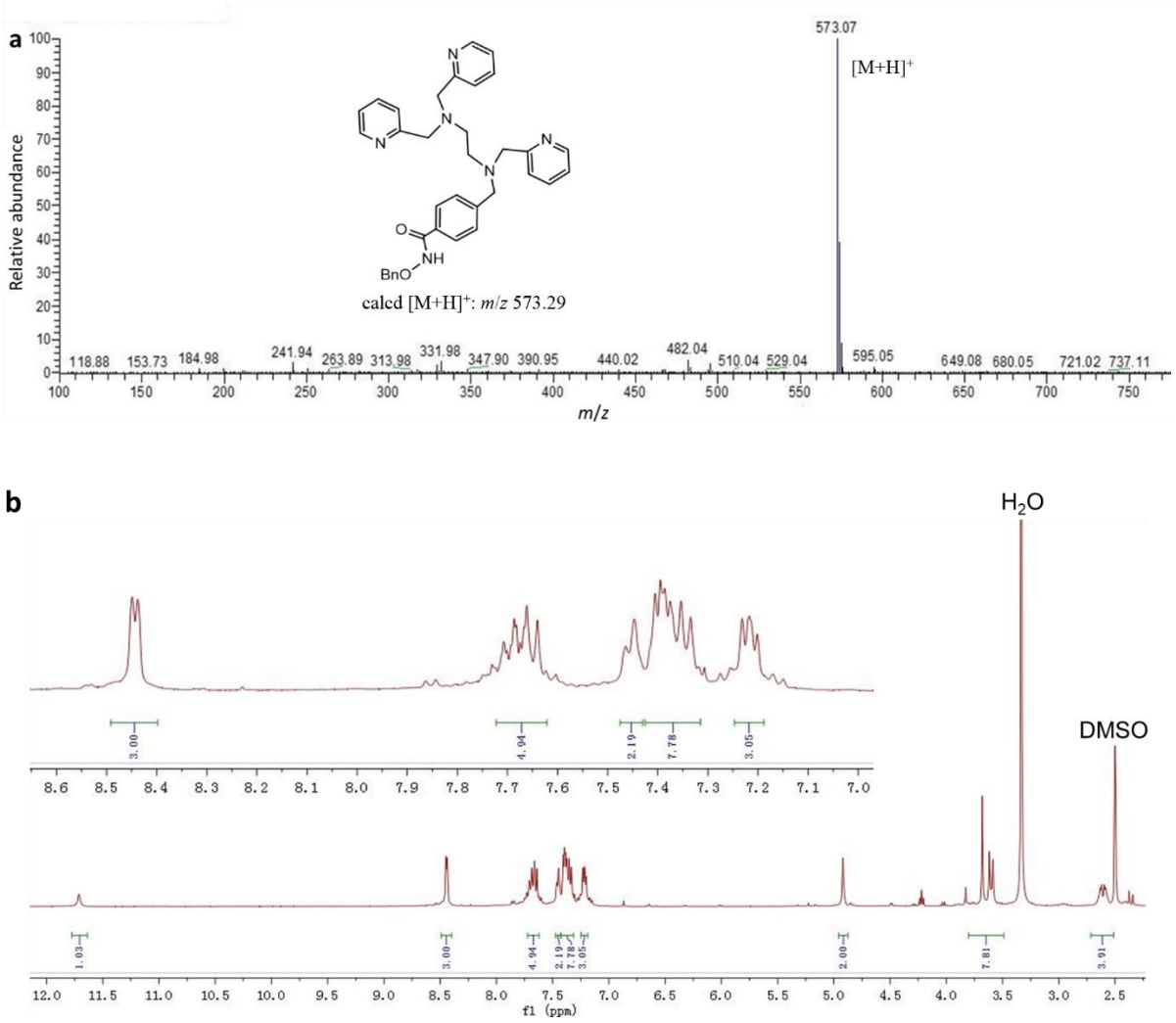

Fig. S4 (a) Mass spectrum and (b) ^{1}H NMR spectrum for product **3** in DMSO-d_6.

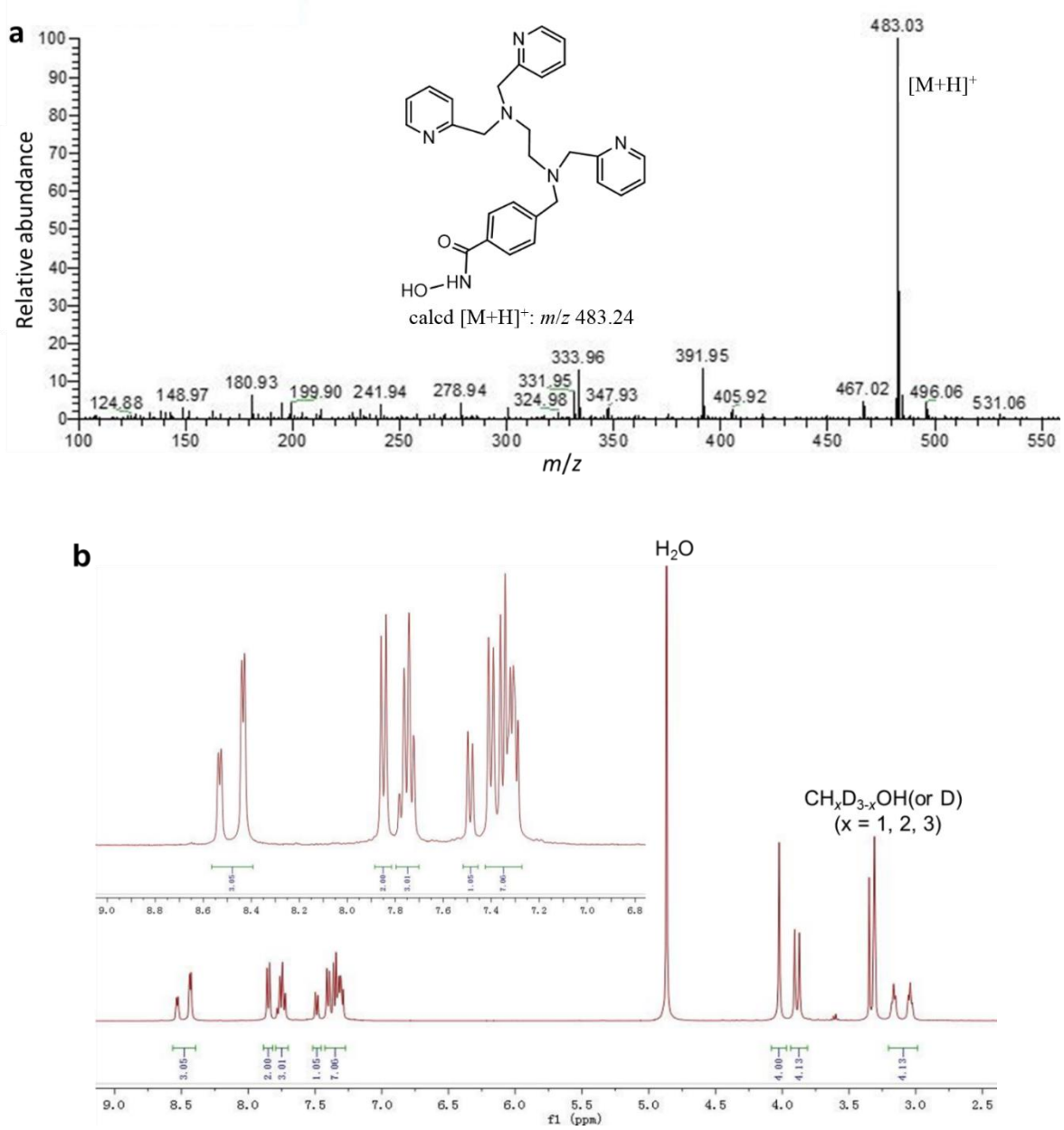

Fig. S5 (a) Mass spectrum and (b) ^{1}H NMR spectrum for ligand $(N_5)^{HA}$ in CD_3OD.

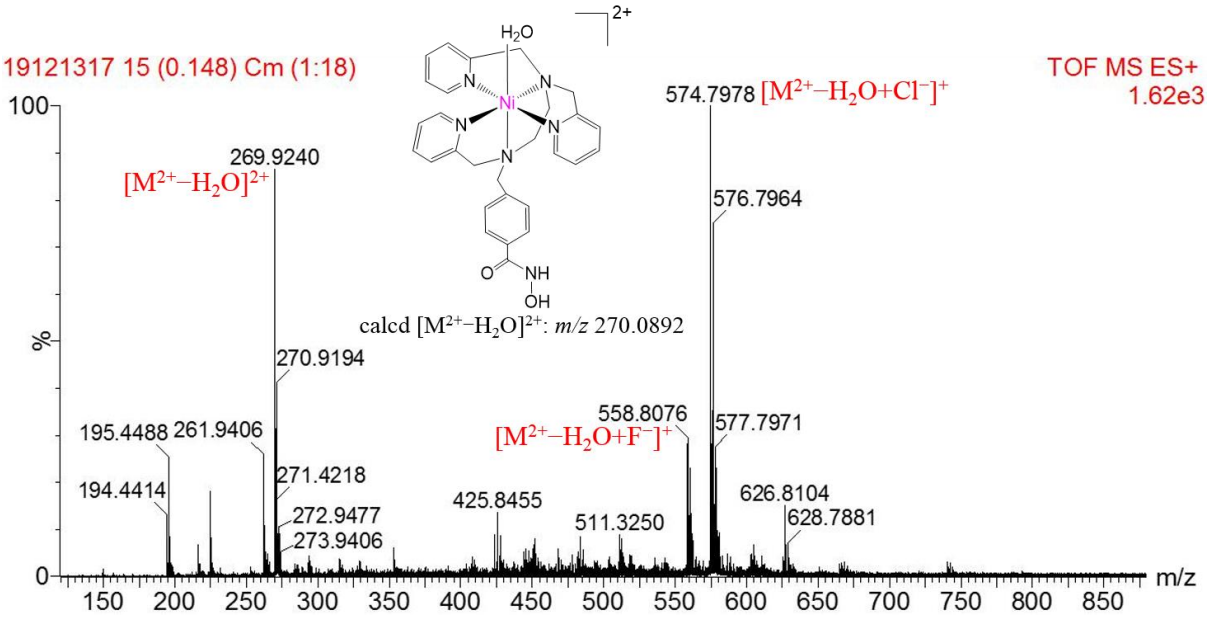

Fig. S6 Mass spectrum for $Ni(N_5)^{HA}$.

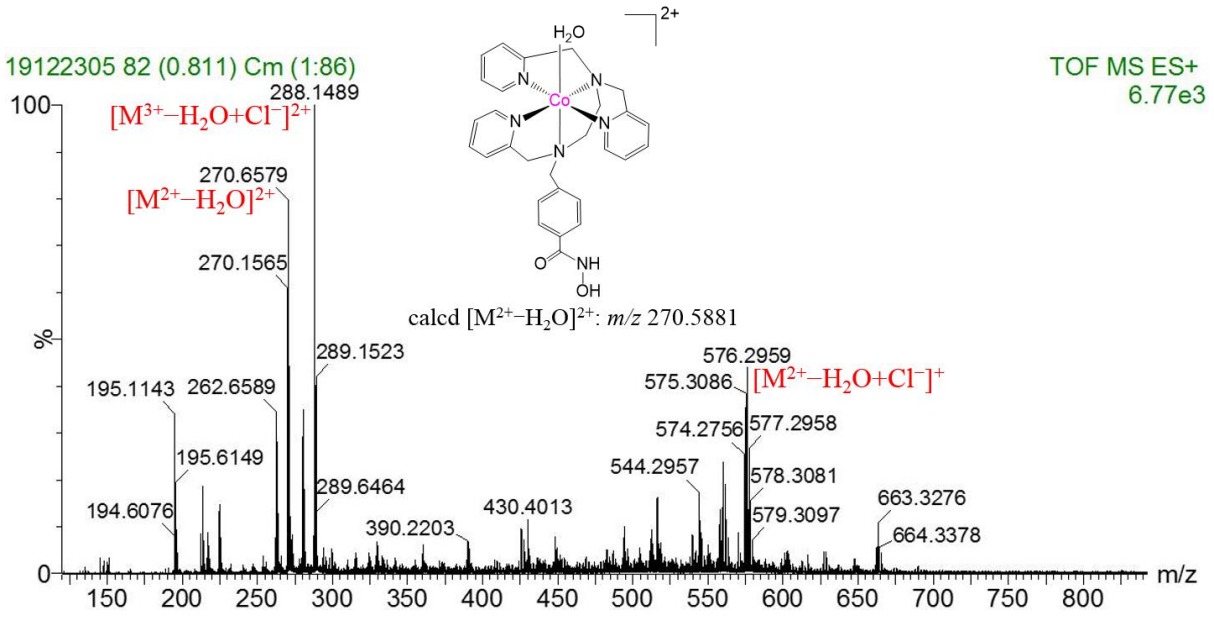

Fig. S7 Mass spectrum for $Co(N_5)^{HA}$.

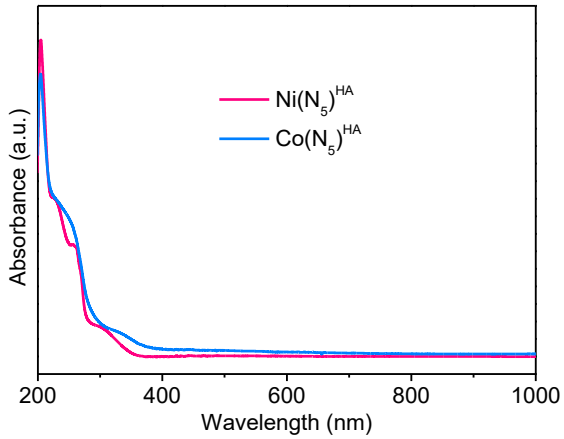

Fig. S8 UV-vis spectra of molecular catalysts (0.05 mM) in MeOH.

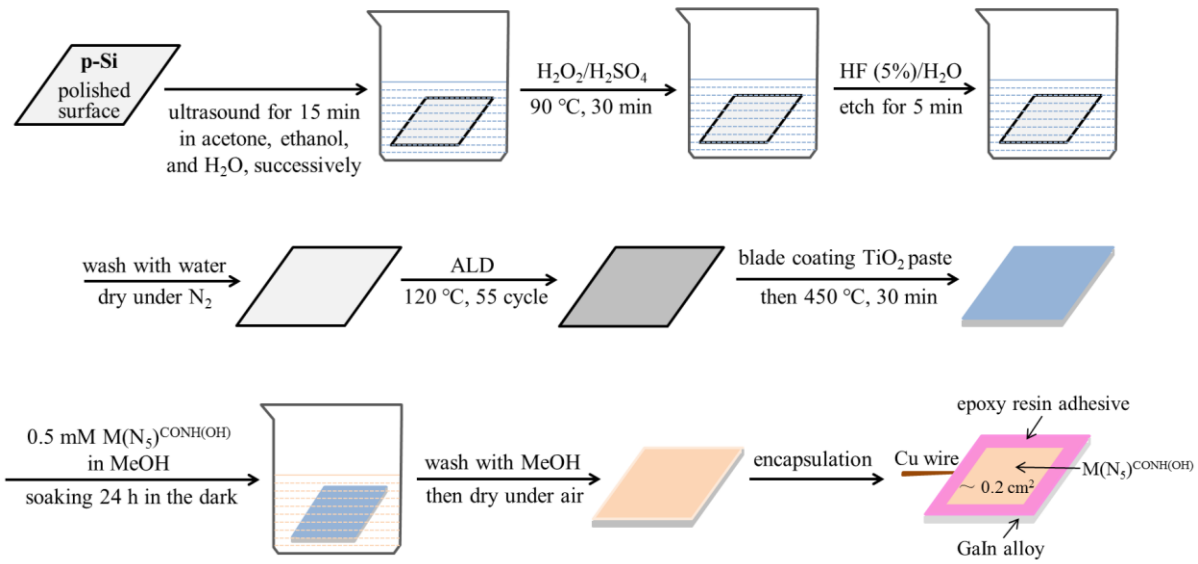

Fig. S9 Schematic illustration for fabrication of p-Si/$TiO_{2(ALD/DB)}$/$M(N_5)^{HA}$ photocathodes.

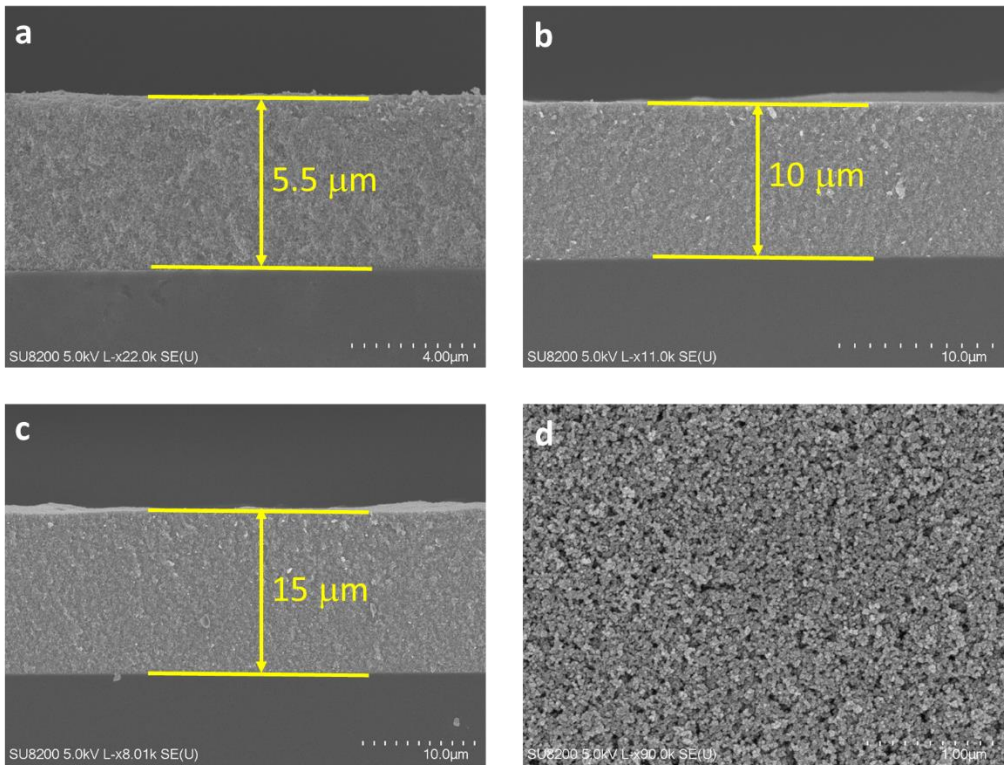

Fig. S10 (a–c) Side-view SEM images of p-Si/$TiO_{2(ALD/DB)}$ with different thicknesses of doctor-blade TiO_2 layers. (d) Top-view SEM image of p-Si/$TiO_{2(ALD/DB)}$.

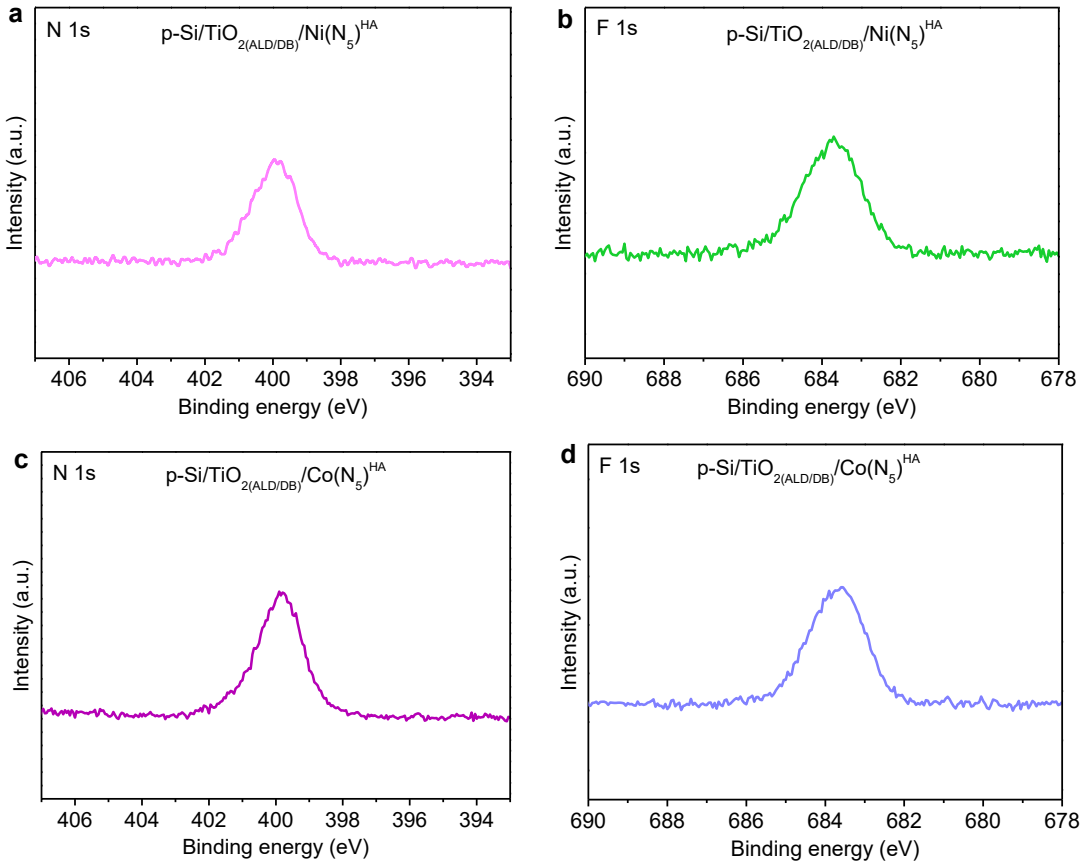

Fig. S11 XPS spectra of N 1s and F 1s for (a,b) as-prepared p-Si/$TiO_{2(ALD/DB)}$/$Ni(N_5)^{HA}$ and (c,d) p-Si/$TiO_{2(ALD/DB)}$/$Co(N_5)^{HA}$.

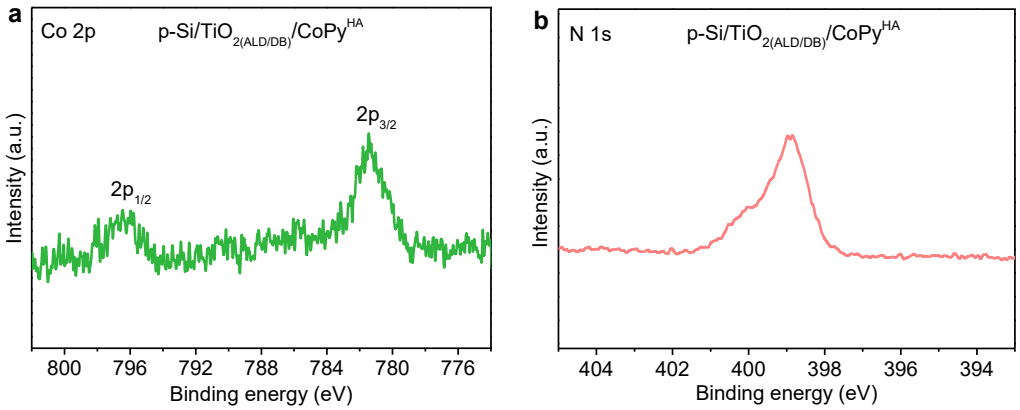

Fig. S12 XPS spectra of (a) Co 2p and (b) N 1s for the as-prepared p-Si/$TiO_{2(ALD/DB)}$/$CoPy^{HA}$ electrode.

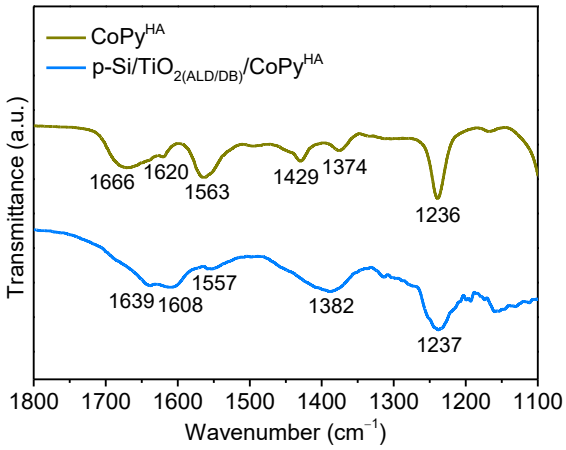

Fig. S13 ATR−FTIR spectra of p-Si/$TiO_{2(ALD/DB)}$/$CoPy^{HA}$ and free $CoPy^{HA}$ (KBr disc).

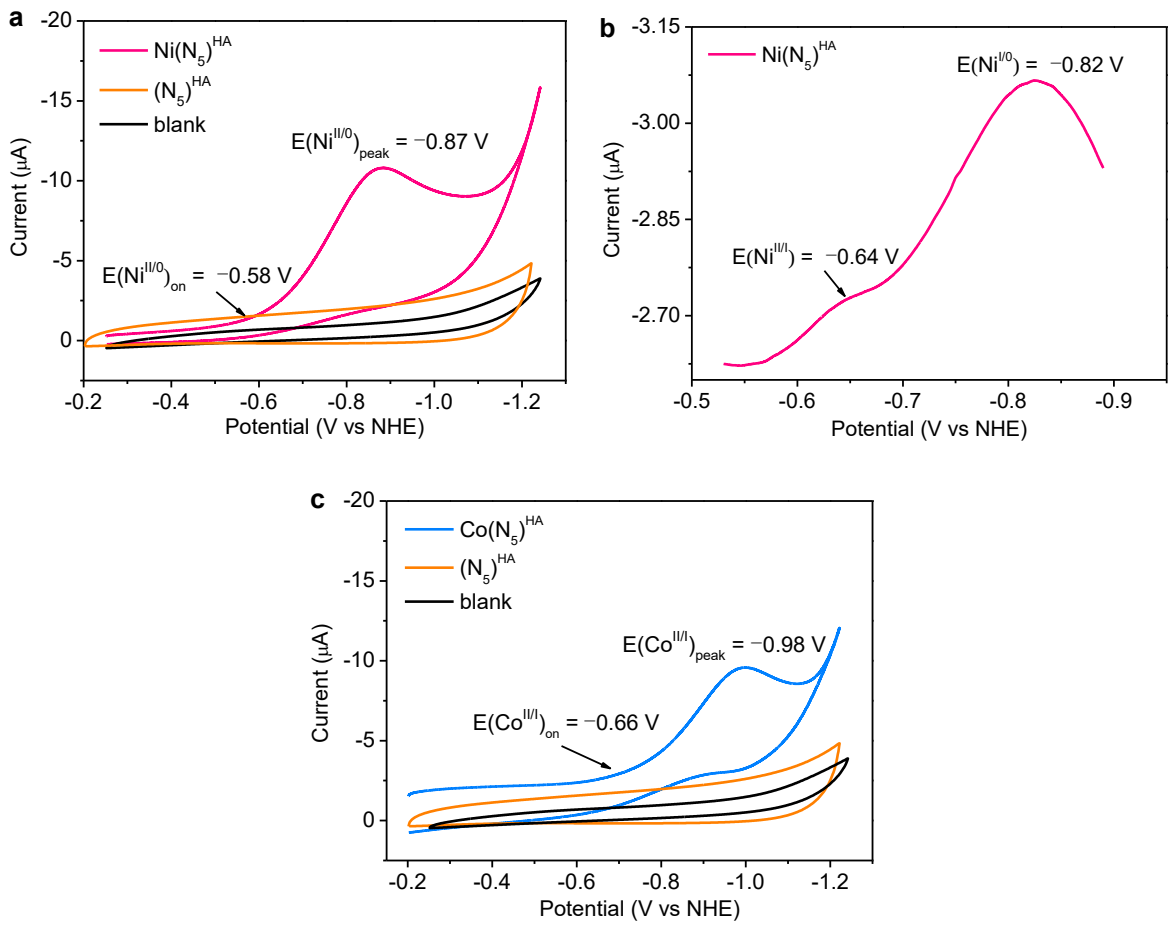

Fig. S14 (a) CVs of $Ni(N_5)^{HA}$ and $(N_5)^{HA}$. (b) DPV of $Ni(N_5)^{HA}$. (c) CVs of $Co(N_5)^{HA}$ and $(N_5)^{HA}$. Measuring conditions: the concentrations of the samples were 1 mM for CVs and 0.5 mM for differential pulse voltammetry (DPV) measurement in 0.1 M potassium hexafluorophosphate at pH 7, with a glassy carbon as the working electrode, a Pt wire as the counter electrode, and a Ag/AgCl as the reference electrode under Ar at 50 mV s^{-1}.

Here potassium hexafluorophosphate buffer was used as the electrolyte because no waves could be observed for the $Ni^{II/I}$, $Ni^{I/0}$, and $Co^{II/I}$ couples when the CVs of N_5-chelated nickel and cobalt catalysts were measured in 0.1 M PBS at pH 7. There is only one broad wave is observed in the LSV of $Ni(N_5)^{HA}$ (Fig. S14a). The further DPV measurement (Fig. S14b) demonstrates that the broad wave in the LSV of $Ni(N_5)^{HA}$ contains both $Ni^{II/I}$ and $Ni^{I/0}$ couples.

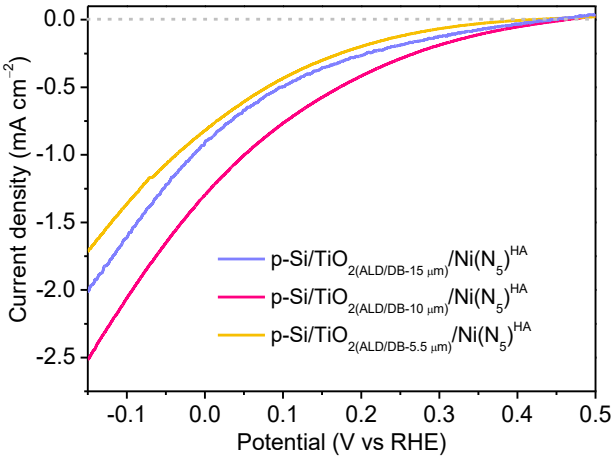

Fig. S15 LSVs of p-Si/$TiO_{2(ALD/DB)}$/Ni$(N_5)^{HA}$ with different thicknesses of the doctor-blade TiO_2 layer in 0.1 M PBS at pH 7 under illumination at 10 mV s^{-1}.

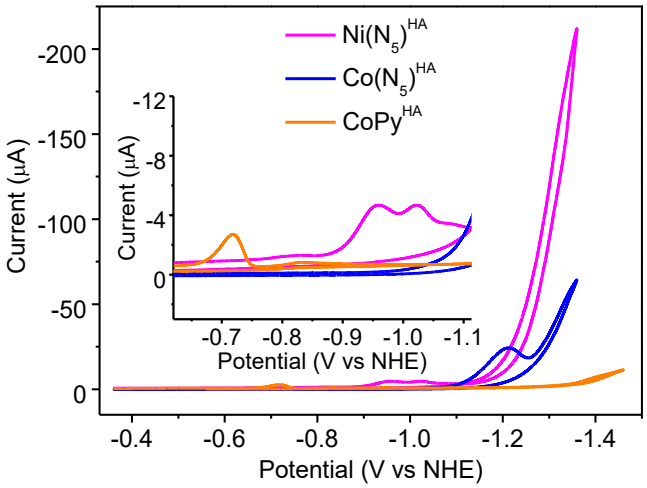

Fig. S16 Cyclic voltammograms of $Ni(N_5)^{HA}$, $Co(N_5)^{HA}$, and $CoPy^{HA}$ (all in 30 μM) in 1 M PBS at pH 7 with a controlled growth mercury drop electrode as the working electrode, a Pt wire as the counter electrode, and a Ag/AgCl as the reference electrode at a scan rate of 100 mV s^{-1}.

As shown in Fig. S16, the reduction peaks of $Ni(N_5)^{HA}$ appeared at −0.96 and −1.02 V, corresponding to $Ni^{II/I}$ and $Ni^{I/0}$ couples, respectively; besides, the reduction peak of $Co^{II/I}$ was located at −1.21 V for $Co(N_5)^{HA}$ and −0.72 V for $CoPy^{HA}$. The higher current of the $Co^{II/I}$ reduction peak for $Co(N_5)^{HA}$ compared to the peak current of $Ni^{II/I}$ and $Ni^{I/0}$ couples for $Ni(N_5)^{HA}$ is due to the overlap of the $Co^{II/I}$ reduction peak with the electrocatalytic current. The reduction peaks of functionalized $Ni(N_5)^{HA}$ and $Co(N_5)^{HA}$ are about 30 and 10 mV, respectively, more positive than that of the corresponding non-functionalized complex,[S3] due to the electron-withdrawing effect of the anchoring group. Accordingly, the catalytic onset potentials were −1.12, about −1.21, and −1.38 V for $Ni(N_5)^{HA}$, $Co(N_5)^{HA}$, and $CoPy^{HA}$, respectively. It is clear that $Ni(N_5)^{HA}$ has much higher catalytic activity than $Co(N_5)^{HA}$ and $CoPy^{HA}$ catalysts for electrochemical HER, which is consistent with the PEC activities of the photocathodes modified by these molecular catalysts (Fig. 3).

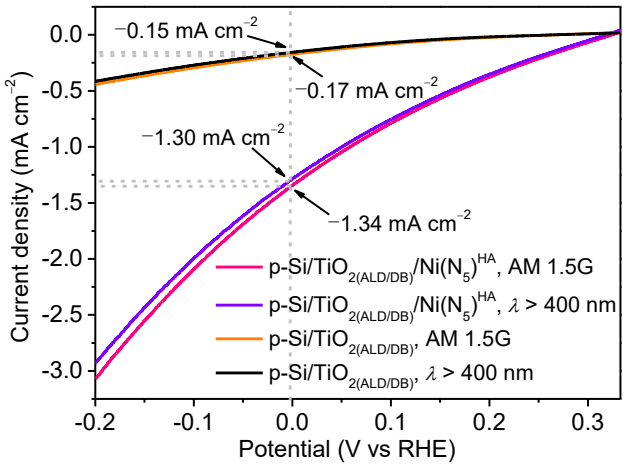

Fig. S17 LSVs of p-Si/$TiO_{2(ALD/DB)}$/$Ni(N_5)^{HA}$ and bare p-Si/$TiO_{2(ALD/DB)}$ in pH 7 PBS (0.1 M) under irradiation with an AM 1.5G filter or a λ > 400 nm cutoff filter at 10 mV s^{-1}.

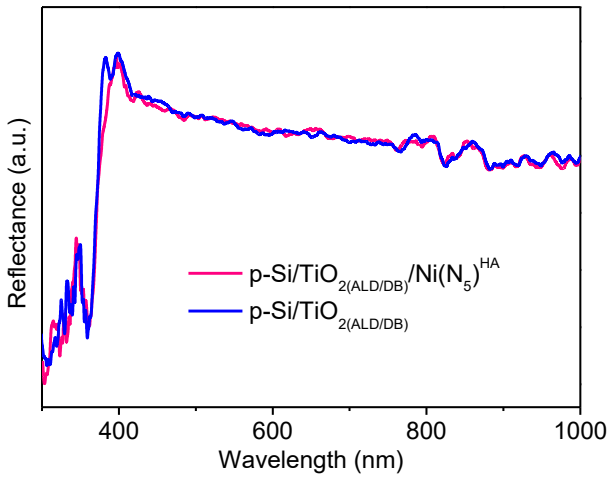

Fig. S18 UV–vis reflectance spectra of p-Si/$TiO_{2(ALD/DB)}$/$Ni(N_5)^{HA}$ and bare p-Si/$TiO_{2(ALD/DB)}$.

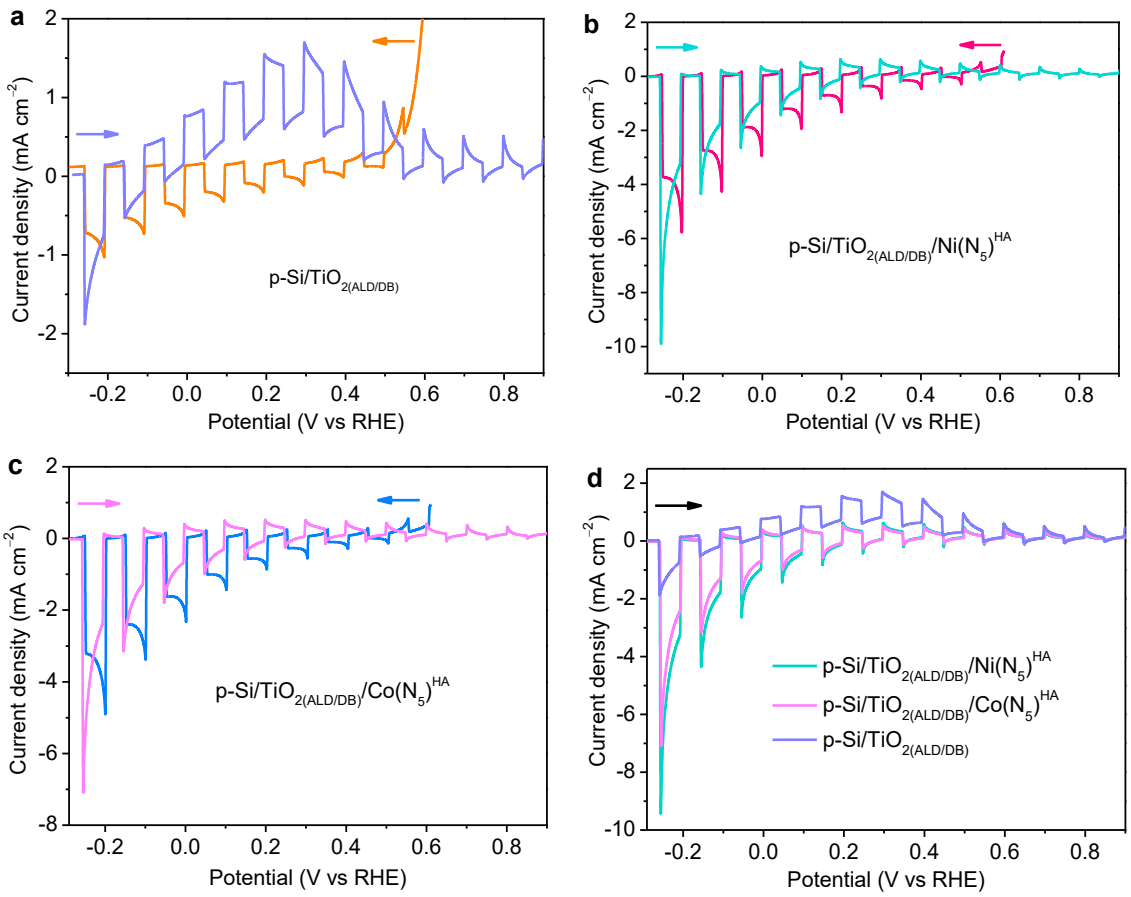

Fig. S19 LSVs of (a) p-Si/TiO$_{2(ALD/DB)}$, (b) p-Si/TiO$_{2(ALD/DB)}$/Ni(N$_5$)^{HA}, and (c) p-Si/TiO$_{2(ALD/DB)}$/Co(N$_5$)^{HA} in 0.1 M PBS at pH 7 under chopped irradiation with scanning first in reducing direction and then in oxidizing direction at 10 mV s^{-1}. (d) LSVs of p-Si/TiO$_{2(ALD/DB)}$/M(N$_5$)^{HA} and bare p-Si/TiO$_{2(ALD/DB)}$ under chopped illumination with scanning in oxidizing direction at 10 mV s^{-1}.

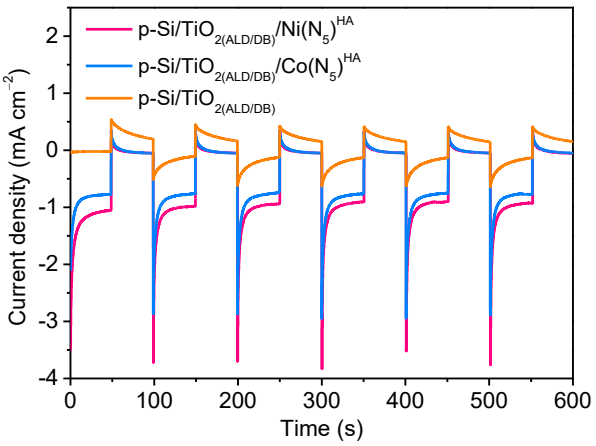

Fig. S20 *j*–*t* plots of p-Si/$TiO_{2(ALD/DB)}$/$M(N_5)^{HA}$ and bare p-Si/$TiO_{2(ALD/DB)}$ in 0.1 M PBS at pH 7 under illumination at 0 V.

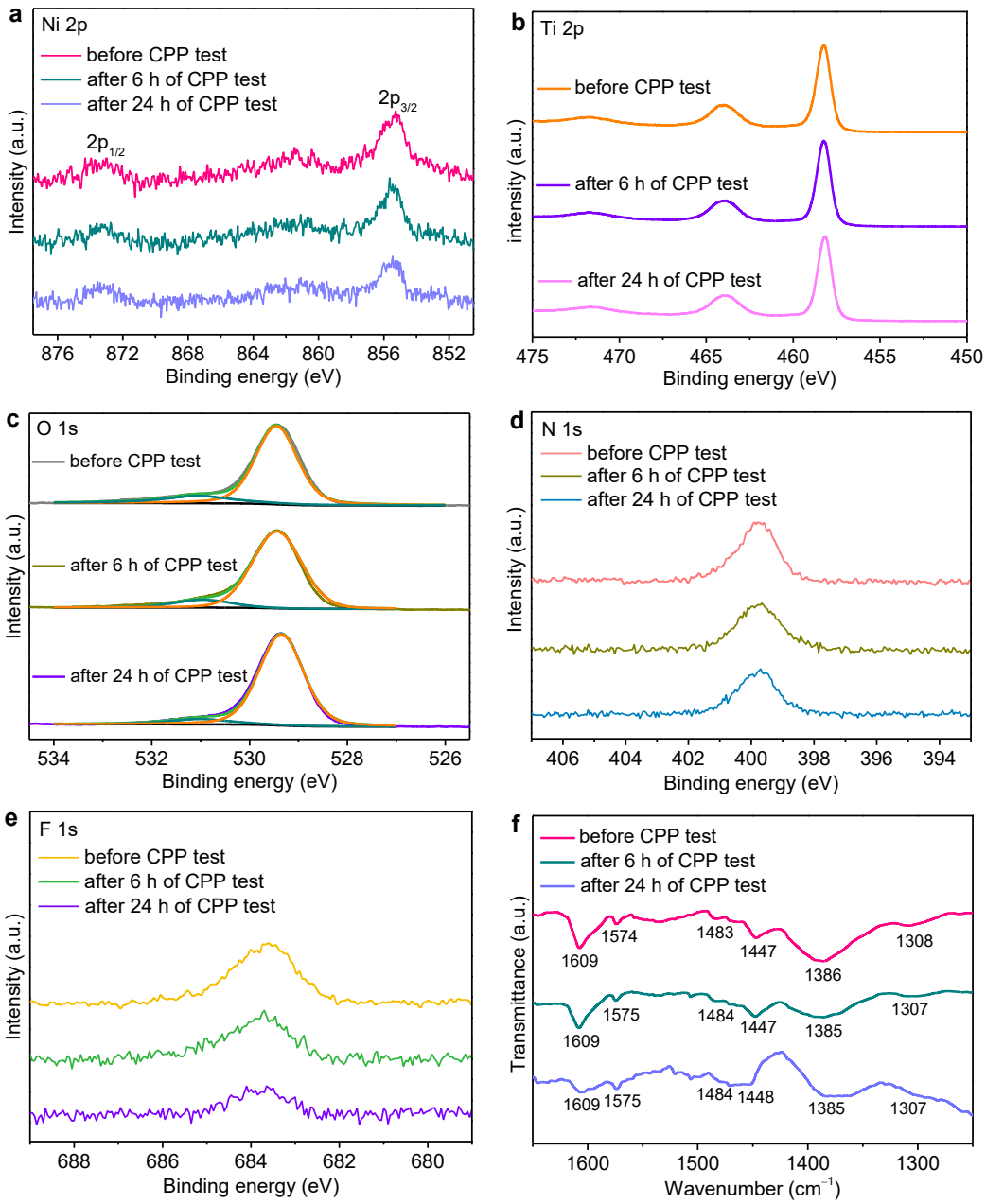

Fig. S21 XPS spectra of (a) Ni 2p, (b) Ti 2p, (c) O 1s, (d) N 1s, (e) F 1s and (f) ATR−FTIR spectra for p-Si/$TiO_{2(ALD/DB)}$/$Ni(N_5)^{HA}$ before and after used for 6 and 24 h of CPP tests.

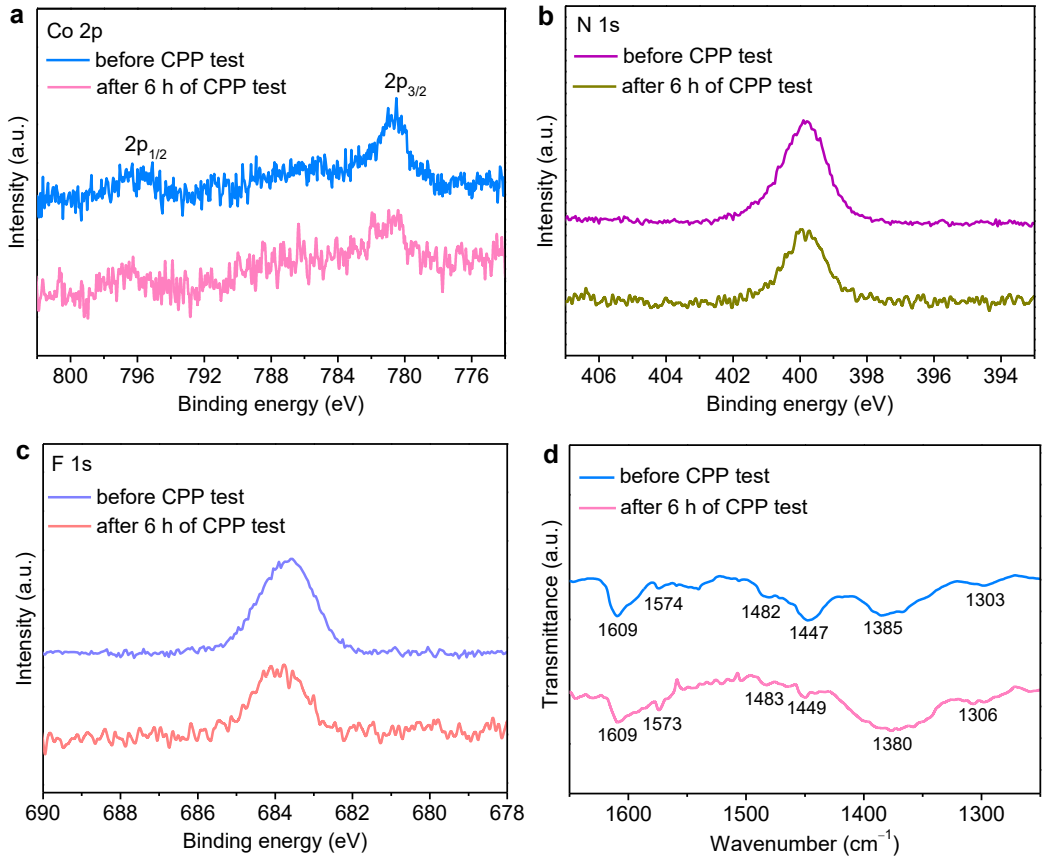

Fig. S22 XPS spectra of (a) Co 2p, (b) N 1s, (c) F 1s, and (d) ATR−FTIR spectra for p-Si/$TiO_{2(ALD/DB)}$/$Co(N_5)^{HA}$ before and after used for 6 h of CPP test.

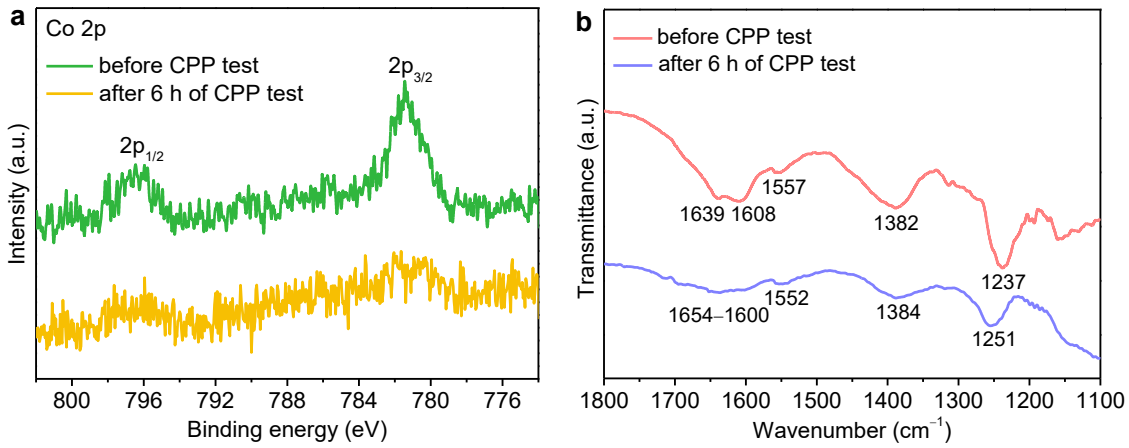

Fig. S23 (a) XPS spectra of Co 2p and (b) ATR−FTIR spectra for p-Si/$TiO_{2(ALD/DB)}$/$CoPy^{HA}$ before and after used for 6 h of CPP test.

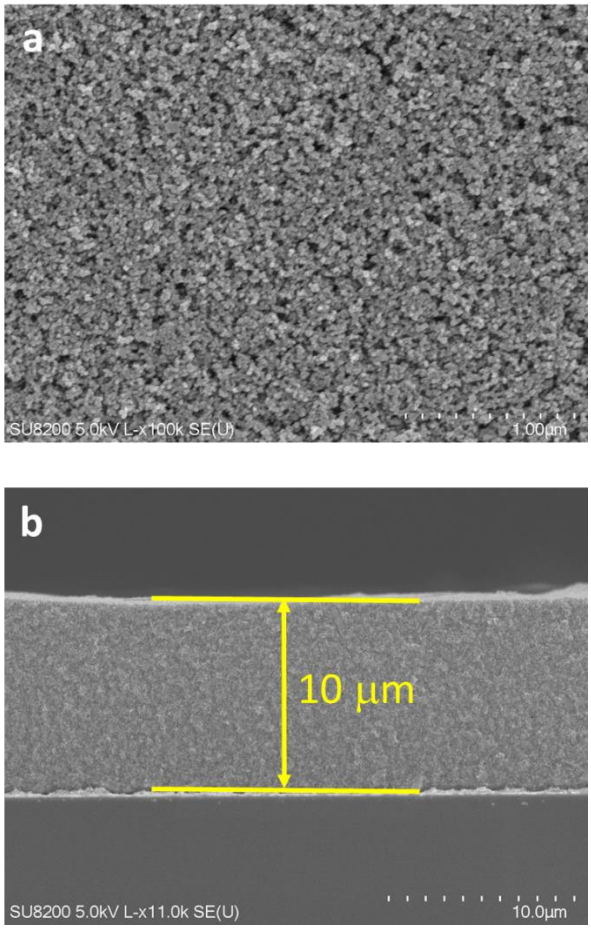

Fig. S24 (a) Top- and (b) side-view SEM images of p-Si/$TiO_{2(ALD/DB)}$/Ni(N_5)^{HA} after 24 h of CPP test.

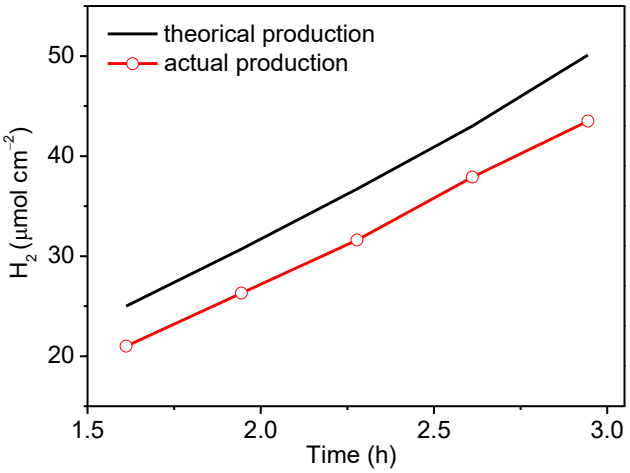

Fig. S25 Plot of the amount of evolved hydrogen of p-Si/$TiO_{2(ALD/DB)}$/Ni(N_5)^{HA} for PEC H_2 production in 0.1 M PBS at pH 7 under AM 1.5G illumination at 0 V.

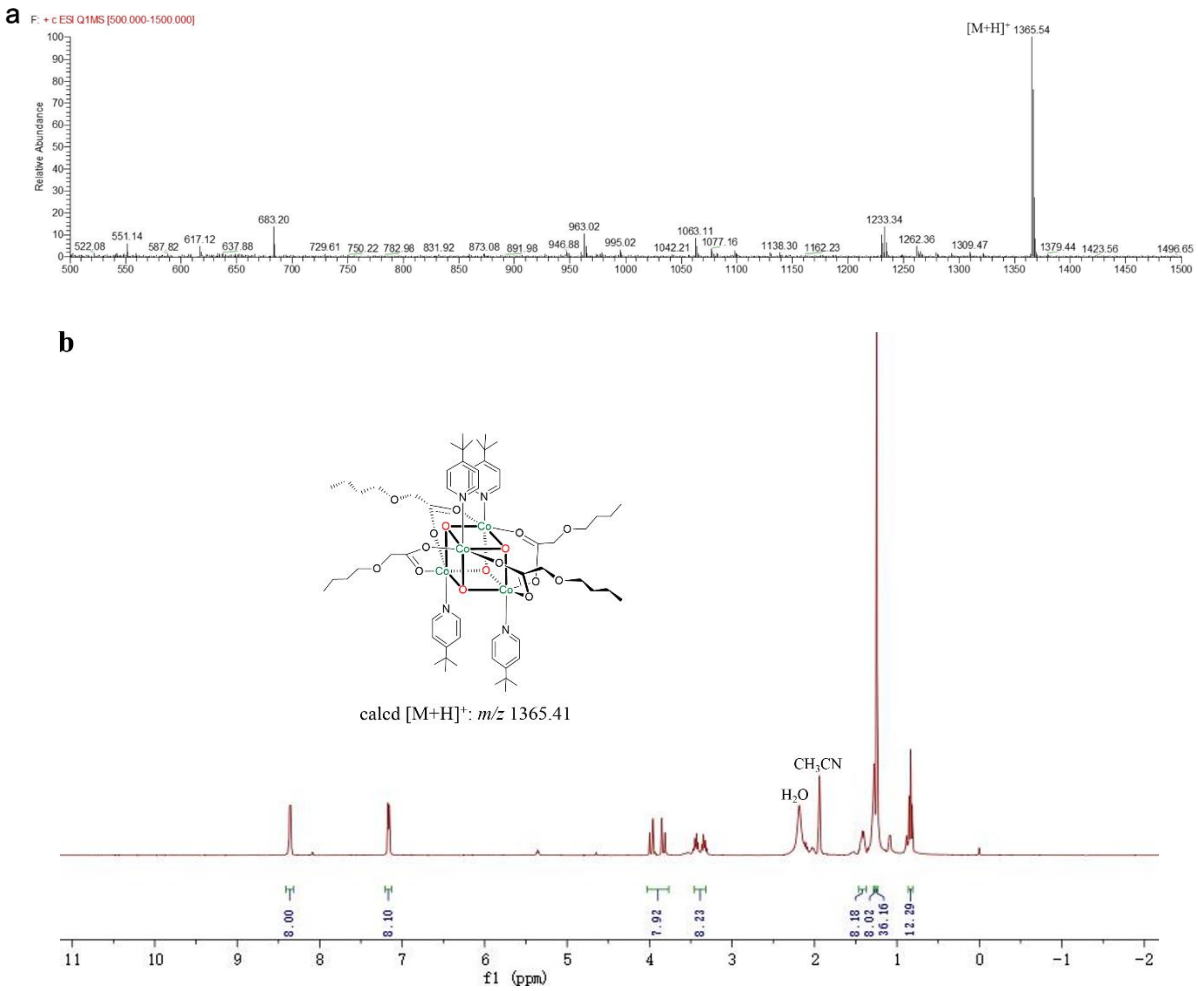

Fig. S26 (a) Mass spectrum and (b) ^{1}H NMR spectrum for the Co_4O_4-OC_4H_9 molecular catalyst in CD_3CN.

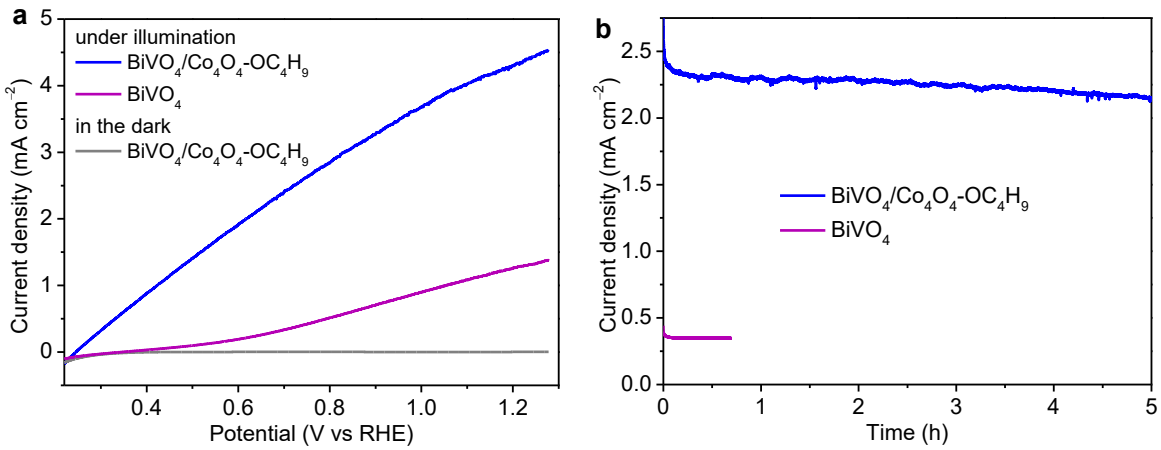

Fig. S27 (a) LSV curves of $BiVO_4/Co_4O_4$-OC_4H_9 and bare $BiVO_4$ under illumination (AM 1.5G, 100 mW cm^{-2}) at 10 mV s^{-1}. (b) Long-time CPP curves for $BiVO_4/Co_4O_4$-OC_4H_9 and bare $BiVO_4$ in 0.1 M BBS (pH = 9) at 0.7 V under illumination for 5 h.

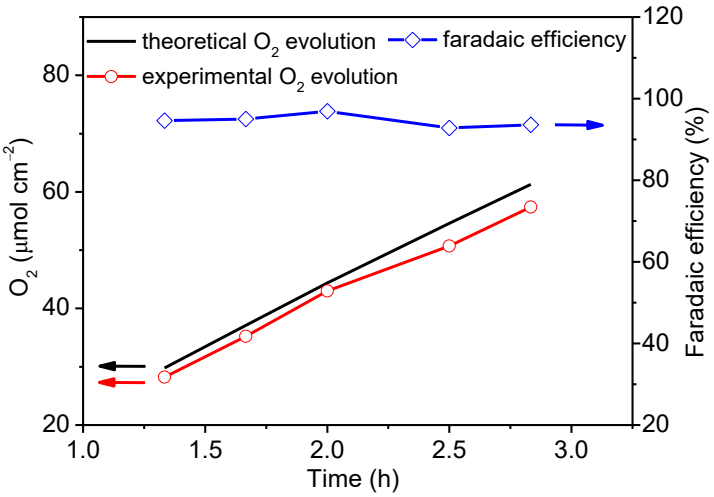

Fig. S28 Plots of theoretical and experimental O_2 evolution and faradaic efficiency for $BiVO_4/Co_4O_4$-OC_4H_9 in 0.1 M BBS (pH = 9) at 0.7 V under AM 1.5G illumination for 2.8 h.

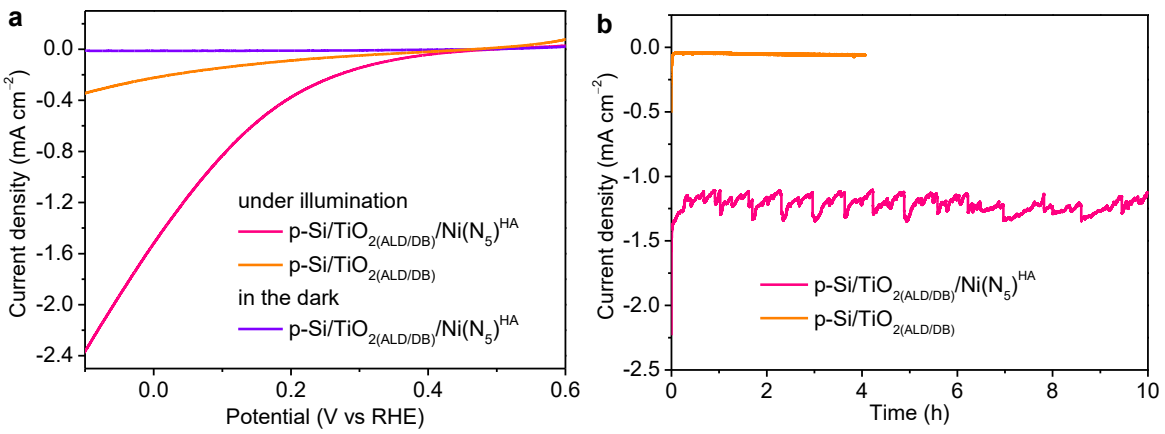

Fig. S29 (a) LSV curves of p-Si/$TiO_{2(ALD/DB)}$/Ni$(N_5)^{HA}$ and bare p-Si/$TiO_{2(ALD/DB)}$ under AM 1.5G illumination at 10 mV s^{-1}. (b) Long-time CPP curves for p-Si/$TiO_{2(ALD/DB)}$/Ni$(N_5)^{HA}$ and bare p-Si/$TiO_{2(ALD/DB)}$ in 0.1 M BBS at pH 9 under illumination at 0 V for 10 h.

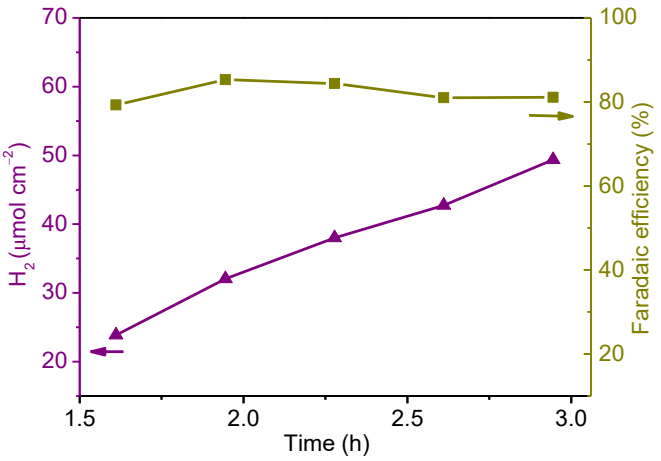

Fig. S30 Plots of the amount of evolved hydrogen and faradaic efficiency for p-Si/$TiO_{2(ALD/DB)}$/Ni$(N_5)^{HA}$ in 0.1 M BBS (pH = 9) at 0 V under AM 1.5G illumination for 3 h.

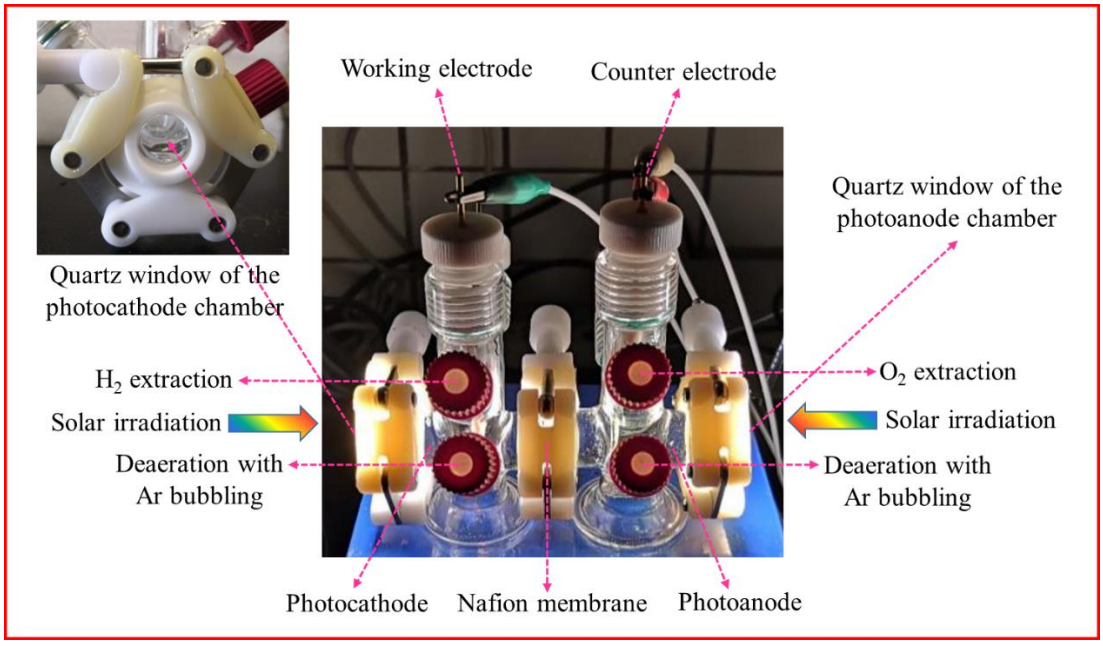

Fig. S31 Photos for the Z-scheme PEC cell assembled by coupling the p-Si/$TiO_{2(ALD/DB)}$/$Ni(N_5)^{HA}$ photocathode with a $BiVO_4$/Co_4O_4-OC_4H_9 photoanode for unbiased overall water splitting.

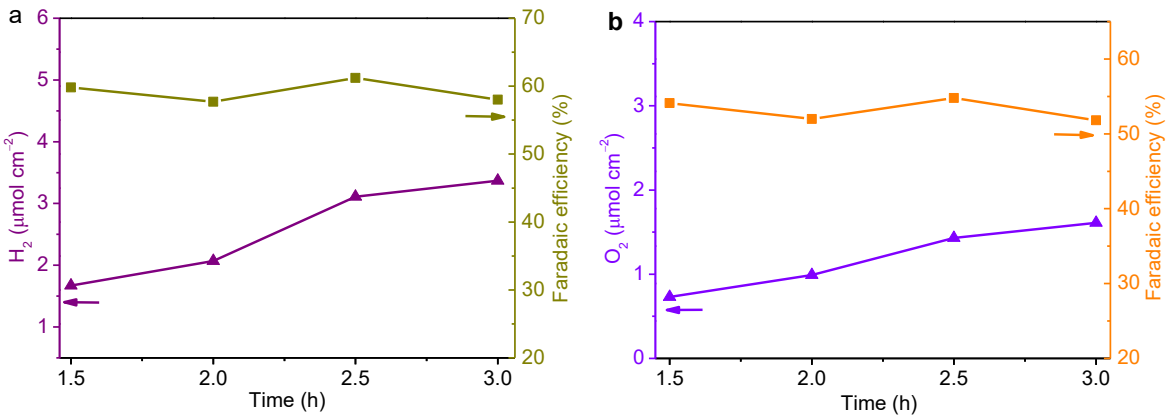

Fig. S32 Plots of the amounts of evolved (a) H_2 and (b) O_2, and the corresponding faradaic efficiencies for the assembled noble-metal-free hybrid PEC cell in 3 h of CPP test at 0 V under AM 1.5G illumination in 0.1 M BBS at pH 9.

Table S1 Amounts of loaded molecular catalysts on the as-prepared photocathodes determined by ICP-OES analysis

Photocathode	Amount of immobilized catalyst (nmol cm^{-2})
p-Si/$TiO_{2(ALD/DB)}$/Ni(N_5)^{HA}	33.0 ± 0.2
p-Si/$TiO_{2(ALD/DB)}$/Co(N_5)^{HA}	30.6 ± 0.9
p-Si/$TiO_{2(ALD/DB)}$/CoPy^{HA}	41.8 ± 1.0
FTO/$TiO_{2(DB)}$/Ni(N_5)^{HA}	11.1 ± 0.1
FTO/$TiO_{2(DB)}$/Co(N_5)^{HA}	11.8 ± 0.2
FTO/$TiO_{2(DB)}$/CoPy^{HA}	11.5 ± 0.2

Table S2 Photocurrent density at 0 V and onset potential of tested hybrid photocathodes in 0.1 M PBS at pH 7

Photocathode	$J_{(0\ V)}$ (mA cm^{-2})	E_{on} (at J = −10 μA cm^{-2}) (V vs RHE)
p-Si/TiO$_{2(ALD/DB)}$/Ni(N$_5$)^{HA}	−1.31	0.45
p-Si/TiO$_{2(ALD/DB)}$/Ni(N$_5$)^{HA}	−1.54 [a]	0.47 [a]
p-Si/TiO$_{2(ALD/DB)}$/Co(N$_5$)^{HA}	−1.12	0.41
p-Si/TiO$_{2(ALD/DB)}$/CoPy^{HA}	−0.42	0.34
p-Si/TiO$_{2(ALD/DB)}$	−0.17	0.21
p-Si/TiO$_{2(ALD/DB)}$	−0.21[a]	0.36 [a]

[a] Measured in 0.1 M BBS at pH 9.

Table S3 PEC data for reported molecular catalyst-modified p-type narrow-band-gap planar semiconductor hybrid photocathodes for hydrogen evolution in aqueous solutions

Photocathode	E_{on} (V vs RHE) [a]	$J_{(0\ V)}$ (mA cm^{-2}) [a]	Stability in CPP [b] (% loss of photocurrent)	TON [b]	TOF [b] (s^{-1})	Electrolyte (pH)	Ref.
GaP-PVP/cobaloxime	0.5	−1.1	18% loss after 15 min [c]	n/a	n/a	0.1 M acetate (pH 4.5)	S7
GaP-PVP/cobaloxime	0.72	−0.92	~ 10% loss after 5 min [d]	n/a	n/a	0.1 M phosphate (pH 7)	S8
GaP-PVP/cobaloxime	0.61	−1.3	27% loss after 1 h	n/a	2.4	0.1 M phosphate (pH 7)	S9
GaP(111)-PVI/cobaloxime	0.65	−0.89	13% loss after 55 min	n/a	1.94	0.1 M phosphate (pH 7)	S10
GaP-PVP/cobaloxime	0.76	−2.7	17% loss after 5 min [d]	n/a	n/a	1 M phosphate (pH 7)	S11
GaP/Co-porphyrin	0.55	−1.31	< 10% loss after 4 h	n/a	≥ 3.9	0.1 M phosphate (pH 7)	S12
$GaInP_2/TiO_2$/cobaloxime/TiO_2	0.7	−9	5% loss after 20 min	1.39×10^5 (20 h)	1.9	0.1 M NaOH (pH 13)	S13
InP/$Fe_2S_2(CO)_6$	0.51	-4.5×10^{-4}	n/a	n/a	n/a	0.1 M $NaBF_4$ (pH 7) [e]	S14
Si/InP/$Fe_2S_2(CO)_6$	0.2	−1.2 [f]	negligible loss after 0.7 h	n/a	n/a	0.1 M H_2SO_4 (pH 1)	S15
$CuFe_xO_y$/cobaloxime	0.8	–	100% loss in 8 min [g]	57 (20 min)	0.05	0.2 M phosphate (pH 6.7)	S16
P3HT:PCBM/cobaloxime	n/a	−0.002	n/a	n/a	n/a	0.1 M acetate (pH 4.5)	S17
Si/ferrocenophane	0.25	n/a	n/a	n/a	n/a	1 M $HClO_4$ (pH 0) [h]	S18
Si/mesoTiO_2/NiP	0.4	−0.34	50% loss after 8 h	~1000 (24 h)	~0.011	0.1 M acetate (pH 4.5) [i]	S19
Si/mesoTiO_2/CoP	0.36	−0.33	100% loss after 0.5 h	~10 (4 h)	6.94×10^{-4}	0.1 M acetate (pH 4.5) [i]	S19
p-Si/$TiO_{2(ALD)}$/$TiO_{2(SC)}$/$CoC_{11}P$/$TiO_{2(ALD)}$	0.47	−1.25	24% loss after 1 h	260 (1 h)	0.071	1 M phosphate (pH 7)	S20
p-Si/$TiO_{2(ALD)}$/$TiO_{2(SC)}$/$CoC_{11}P$	0.09	−0.5	negligible loss after 1 h	n/a	n/a	1 M phosphate (pH 7)	S20
Si/TiO_2/$CoPy^{HA}$	0.32	−0.32	3% loss after 6 h	736 (5.5 h)	0.037	0.1 M borate (pH 9) [i]	S1
p-Si/$TiO_{2(ALD/DB)}$/$CoPy^{HA}$	0.34	−0.42	16% loss after 6 h	–	–	0.1 M phosphate (pH 7)	This work
p-Si/$TiO_{2(ALD/DB)}$/$Co(N_5)^{HA}$	0.41	−1.12	negligible loss after 6 h	–	–	0.1 M phosphate (pH 7)	
p-Si/$TiO_{2(ALD/DB)}$/$Ni(N_5)^{HA}$	0.45	−1.31	negligible loss after 24 h	1318 (3 h)	0.122	0.1 M phosphate (pH 7)	
p-Si/$TiO_{2(ALD/DB)}$/$Ni(N_5)^{HA}$	0.47	−1.54	negligible loss after 10 h	1497 (3 h)	0.141	0.1 M borate (pH 9)	

[a] LSV measurements under 100 mW cm^{-2}, AM 1.5G illumination. [b] At 0 V except as otherwise noted. [c] At −0.12 V. [d] At 0.17 V. [e] LED, λ = 395 nm. [f] At −0.26 V. [g] Under illumination of 65 mW cm^{-2}, λ 400–700 nm at 0.4 V. [h] Xe lamp, 870 mW cm^{-2}. [i] 100 mW cm^{-2}, AM 1.5G, λ > 400 nm. The rest was carried out under illumination of 100 mW cm^{-2}, AM 1.5G.

Table S4 ICP-OES analysis data for the amounts of loaded catalysts on electrode surface and of the M^{n+} species in electrolyte after CPP experiments

Photocathode	Amount of M^{n+} species in electrolyte after 6 h of CPP test (nmol)[a]	Amount of Ni^{n+} species in electrolyte after 24 h of CPP test (nmol)	Amount of catalyst on electrode surface before CPP test (nmol cm^{-2})
p-Si/$TiO_{2(ALD/DB)}$/$Ni(N_5)^{HA}$	0.3 ± 0.1	0.9 ± 0.2	33.0 ± 0.2
p-Si/$TiO_{2(ALD/DB)}$/$Co(N_5)^{HA}$	0.8 ± 0.1	—	30.6 ± 0.9
p-Si/$TiO_{2(ALD/DB)}$/$CoPy^{HA}$	5.7 ± 0.3	—	41.8 ± 1.0

[a] M = Ni, Co.

Table S5 Summary of PEC data reported for molecular PEC cells toward overall water splitting in aqueous solution

PEC cell	E_{int} (V) [a]	$\lvert J_{(0\ V)}\rvert$ (mA cm^{-2}) [b]	CPP duration (loss%) of photocurrent	H_2 (μmol cm^{-2})	TON_{H_2}	FE_{H_2} (%)	O_2 (μmol cm^{-2})	FE_{O_2} (%)	STH (%) @ applied bias	Electrolyte (pH)	Ref.
IO-ITO/H_2ase‖IO-TiO_2/dpp/P_{OS}/PSII [c]	0.08	< 0.03	1 h (96.4%)	0.06	n/a	76	n/a	n/a	0.0047 @ 0 V	$CaCl_2$ (20 mM), $MgCl_2$ (15 mM), KCl (50 mM), MES (40 mM) (pH 6.5)	S21
$CuGaO_2$/RBG174-dye/cobaloxime‖TaON/CoO_x [d]	0.6	0.005	2 h (50%)	0.13	< 346	87	0.06	88	0.0054 @ 0 V	0.05 M phosphate (pH 7)	S22
NiO/P1-dye/cobaloxime‖TiO_2/L0-dye/Ru-pdc [e]	n/a	0.07	1.7 h (80%)	0.33	n/a	55	n/a	n/a	0.0051 @ 0 V	0.05 M phosphate (pH 7)	S23
NiO/RuP/cobaloxime‖TiO_2/RuP/Ru-pdc [e]	n/a	0.01	3.3 min (30%)	n/a	n/a	n/a	n/a	n/a	n/a	0.07 M phosphate (pH 7)	S24
p-Si/Ti/TiO_2/PDI′/NiCt‖SnO_2/TiO_2/RuP_2-RuCt [f]	n/a	0.3	2.5 h (>31%)	n/a	n/a	19−54	n/a	32−73	n/a	0.1 M acetate with 0.9 M $NaClO_4$ (pH 4.5)	S25
NiO/PMI-6T-TPA-dye‖$BiVO_4$ [g]	n/a	0.0027	4 h (0%)	0.16	n/a	80	n/a	n/a	n/a	0.1 M Na_2SO_4 (pH 7)	S26
TiO_2/NiP‖WO_3/FeP [f]	no	~0	1 h (n/a)	1.04 ± 0.29	n/a	53 ± 17	0.61 ± 0.06	61 ± 5	< 0.019 @ 1.1 V	0.1 M Na_2SO_4 (pH 3)	S27
p-Si/$TiO_{2(ALD/DB)}$/$Ni(N_5)^{HA}$‖$BiVO_4$/Co_4O_4-OC_4H_9 [h]	0.28	0.181	5 h (24.8%)	3.37	102	58.7 ± 2.5	1.61	52.6 ± 2.2	0.04 @ 0 V	0.1 M borate (pH 9)	This work

[a] E_{int} represents the potential at the intersection of the *J*–*E* curves of photoanode and photocathode. [b] At zero bias. Test light source and intensity: [c] AM 1.5G, 100 mW cm^{-2}, λ > 420 nm for photoanode; [d] 30 mW cm^{-2}, 650 nm > λ > 460 nm for photocathode and 50 mW cm^{-2}, 650 nm > λ > 400 nm for photoanode; [e] 100 mW cm^{-2}, λ > 400 nm for both photocathode and photoanode; [f] AM 1.5G, 100 mW cm^{-2} for photoanode; [g] 300 W Xe lamp, λ > 420 nm for both photocathode and photoanode; [h] AM 1.5G, 100 mW cm^{-2} for both photocathode and photoanode.

References

S1 L. Gong, H. Yin, C. Nie, X. Sun, X. Wang and M. Wang, *ACS Appl. Mater. Interfaces*, 2019, **11**, 34010–34019.

S2 P. Zhang, M. Wang, F. Gloaguen, L. Chen, F. Quentelb and L. Sun, *Chem. Commun*., 2013, **49**, 9455–9457.

S3 P. Zhang, M. Wang, Y. Yang, D. Zheng, K. Han and L. Sun, *Chem. Commun*., 2014, **50**, 14153–14156.

S4 Y. Wang, F. Li, X. Zhou, F. Yu, J. Du, L. Bai and L. Sun, *Angew. Chem. Int. Ed*., 2017, **56**, 6911–6915.

S5 M. G. Kast, L. J. Enman, N. J. Gurnon, A. Nadarajah and S. W. Boettcher, *ACS Appl. Mater. Interfaces*, 2014, **6**, 22830−22837.

S6 T. W. Kim and K.-S. Choi, *Science*, 2014, **343**, 990−994.

S7 D. Cedeno, A. Krawicz, P. Doak, M. Yu, J. B. Neaton and G. F. Moore, *J. Phys. Chem. Lett*., 2014, **5**, 3222–3226.

S8 A. Krawicz, D. Cedeno and G. F. Moore, *Phys. Chem. Chem. Phys*., 2014, **16**, 15818–15824.

S9 A. M. Beiler, D. Khusnutdinova, S. I. Jacob and G. F. Moore, *Ind. Eng. Chem. Res*., 2016, **55**, 5306–5314.

S10 A. M. Beiler, D. Khusnutdinova, S. I. Jacob and G. F. Moore, *ACS Appl. Mater. Interfaces*, 2016, **8**, 10038–10047.

S11 A. Krawicz, J. Yang, E. Anzenberg, J. Yano, I. D. Sharp and G. F. Moore, *J. Am. Chem. Soc*., 2013, **135**, 11861–11868.

S12 D. Khusnutdinova, A. M. Beiler, B. L. Wadsworth, S. I. Jacob and G. F. Moore, *Chem. Sci*., 2017, **8**, 253–259.

S13 J. Gu, Y. Yan, J. L. Young, K. X. Steirer, N. R. Neale and J. A. Turner, *Nat.*

Mater., 2016, **15**, 456–460.

S14 T. Nann, S. K. Ibrahim, P. M. Woi, S. Xu, J. Ziegler and C. J. Pickett, *Angew. Chem. Int. Ed*., 2010, **49**, 1574–1577.

S15 S. Chandrasekaran, T. J. Macdonald, Y. J. Mange, N. H. Voelcker and T. Nann, *J. Mater. Chem. A*, 2014, **2**, 9478–9481.

S16 C. Tapia, E. Bellet-Amalric, D. Aldakov, F. Boudoire, K. Sivula, L. Cagnone and V. Artero, *Green Chem*., 2020, **22**, 3141–3149.

S17 Y. Chen, H. Chen and H. Tian, *Chem. Commun*., 2015, **51**, 11508–11511.

S18 U. T. Mueller-Westerhoff and A. Nazzal, *J. Am. Chem. Soc*., 1984, **106**, 5381–5382.

S19 J. J. Leung, J. Warnan, D. H. Nam, J. Z. Zhang, J. Willkomm and E. Reisner, *Chem. Sci*., 2017, **8**, 5172–5180.

S20 S. Chandrasekaran, N. Kaeffer, L. Cagnon, D. Aldakov, J. Fize, G. Nonglaton, F. Baleras, P. Mailley and V. Artero, *Chem. Sci.*, 2019, **10**, 4469−4475.

S21 K. P. Sokol, W. E. Robinson, J. Warnan, N. Kornienko, M. M. Nowaczyk, A. Ruff, J. Z. Zhang and E. Reisner, *Nat. Energy*, 2018, **3**, 944−951.

S22 C. D. Windle, H. Kumagai, M. Higashi, R. Brisse, S. Bold, B. Jousselme, M. Chavarot-Kerlidou, K. Maeda, R. Abe, O. Ishitani and V. Artero, *J. Am. Chem. Soc*., 2019, **141**, 9593−9602.

S23 F. Li, K. Fan, B. Xu, E. Gabrielsson, Q. Daniel, L. Li and L. Sun, *J. Am. Chem. Soc*., 2015, **137**, 9153−9159.

S24 K. Fan, F. Li, L. Wang, Q. Daniel, E. Gabrielsson and L. Sun, *Phys. Chem. Chem. Phys*., 2014, **16**, 25234−25240.

S25 B. Shan, M. K. Brennaman, L. Troian-Gautier, Y. Liu, A. Nayak, C. M. Klug, T.-T. Li, R. M. Bullock and T. J. Meyer, *J. Am. Chem. Soc*., 2019, **141**, 10390–10398.

S26 L. Tong, A. Iwase, A. Nattestad, U. Bach, M. Weidelener, G. Götz, A. Mishra, P. Bäuerle, R. Amal, G. G. Wallace and A. J. Mozer, *Energy Environ. Sci*., 2012, **5**, 9472–9475.

S27 T. E. Rosser, M. A. Gross, Y.-H. Lai and E. Reisner, *Chem. Sci*., 2016, **7**, 4024–4035.